Radiative Heat Transfer in Emitting-Absorbing-Scattering Spherical Media

Timothy W. Tong* and Pananjady S. Swathi†
University of Kentucky, Lexington, Kentucky

Radiative heat transfer in spherical media that emit, absorb, and scatter radiation is analyzed. Linear anisotropic scattering is considered. The spherical harmonics method is used to solve the equation of transfer. The *P*-1, *P*-2, *P*-3, *P*-7, and *P*-11 solutions are presented and their accuracy is discussed. Numerical results presented include the radiant heat fluxes at the inner and outer walls of the spherical enclosure and the distribution of the blackbody emissive power in the medium. The effect of scattering on the transfer of radiant energy is illustrated.

Nomenclature

a_j	= angular distribution coefficients in the scattering phase function
e_b	= blackbody emissive power
f	= scattering phase function
F_1, F_2	= constants in the *P*-1 approximation
G_1, G_2	= constants in the *P*-2 approximation
H_1, H_2, H_3, H_4	= constants in the *P*-3 approximation
i	= intensity
i_b	= blackbody intensity
I	= modified Bessel functions of the first kind
K	= modified Bessel functions of the second kind
$P_j(\mu)$	= Legendre polynomial of order j and argument μ
$\dot{Q}$	= volumetric heat generation rate
$\bar{Q}$	= ratio of $\dot{Q}$ to σ_a
$\bar{r}$	= radius vector
T	= absolute temperature
δ_{om}	= Kronecker delta
ϵ_1, ϵ_2	= emissivities of the inner and outer walls, respectively
μ	= cosine of the angle between the direction of the beam and the radius vector
σ_a	= absorption coefficient
σ_s	= scattering coefficient
τ	= optical depth
τ_1, τ_2	= optical depths of the inner and outer walls, respectively
$\psi_m(\tau)$	= expansion function in the spherical harmonics approximation
ω	= single scattering albedo

Introduction

THE growing realization of the importance of radiative heat transfer in participating media has resulted in numerous studies by different investigators in this area. In particular, thermal radiation in planar systems has received the most attention by far. Comparatively little research effort has been devoted towards cylindrical and spherical systems despite their importance in applications such as in nuclear, combustion, and thermal insulation systems. This paper presents an analysis that concerns radiation in emitting-absorbing-scattering spherical media. The objectives of the analysis were to establish some important characteristics about radiative transport in spherical systems and to study the suitability of the spherical harmonics method for analyzing such a problem.

While some publications have appeared on radiative heat transfer in spherical systems, most have dealt only with emitting-absorbing media.[1-6] Sparrow et al.[1] considered a spherical emitting-absorbing gray gas confined between two concentric spheres and presented results for the gas emissive power and the radiant heat flux at the bounding surfaces. Rhyming[2] also investigated a similar problem. The problem in both works was formulated with the gas temperature and the radiant heat flux expressed in terms of integral equations. Differential approximation was used by Dennar and Sibulkin[3] where half-range moments were introduced to reduce the equation of transfer to a set of ordinary differential equations. Bayazitoglu and Higenyi[4] employed the spherical harmonics method to solve the equation of transfer. They obtained the third order (*P*-3) solution and showed good agreement with the integral solution.[2] The first (*P*-1) and second (*P*-2) order solutions were recently presented by Pomraning.[5] Pomraning indicated that, contrary to the traditional belief that the *P*-1 solution was unconditionally superior to the *P*-2 solution, the *P*-2 solution was just as accurate as the *P*-1 solution for predicting the radiant heat flux at the wall of a spherical enclosure.

In this work, the spherical harmonics method was used to solve the equation of transfer governing radiation in emitting-absorbing-scattering spherical media. The analytical *P*-1, *P*-2, and *P*-3 solutions were obtained. Numerical results from the *P*-7 and *P*-11 approximations were used to assess the convergence of the lower order solutions. For the case of no scattering, the results were also checked against those reported by other investigators.[1]

Mathematical Formulation

The physical problem considered is schematically depicted in Fig. 1. Between two diffuse, gray isothermal concentric spheres is a gray medium, which emits, absorbs, and scatters thermal radiation. The medium is considered to have uniform volumetric heat generation. The equation of transfer govern-

Received June 20, 1985; revision submitted Dec. 27, 1985.

*Associate Professor, Department of Mechanical Engineering; currently at the Department of Mechanical and Aerospace Engineering, Arizona State University, Tempe, AZ. Member AIAA.

†Research Assistant, Department of Mechanical Engineering; currently at the Department of Mechanical and Aerospace Engineering, Arizona State University, Tempe, AZ. Student Member AIAA.

ing the intensity in a spherically symmetrical system is

$$\frac{\mu\partial i(\tau,\mu)}{\partial\tau}+\frac{1-\mu^2}{\tau}\frac{\partial i(\tau,\mu)}{\partial\mu}+i(\tau,\mu)=(1-\omega)i_b(T)$$

$$+\frac{\omega}{2}\int_{-1}^{1}f(\mu,\mu')i(\tau,\mu')\mathrm{d}\mu' \tag{1}$$

The optical depth τ and the single scattering albedo ω are defined as

$$\partial\tau\equiv(\sigma_a+\sigma_s)\partial r \tag{2}$$

$$\omega\equiv\frac{\sigma_s}{\sigma_a+\sigma_s} \tag{3}$$

The scattering phase function f is expressed as

$$f(\mu,\mu')=\sum_{j=0}^{\infty}(2j+1)a_jP_j(\mu)P_j(\mu'),\quad a_0=1 \tag{4}$$

The values of a_j are dependent on the type of scattering being modeled, and some typical values are shown in Table 1. The conservation equation for energy when conduction and convection are absent is

$$\dot{Q}=4\pi\sigma_a i_b(T)-2\pi\sigma_a\int_{-1}^{1}i(\tau,\mu)\mathrm{d}\mu \tag{5}$$

In the spherical harmonics method, the intensity is expanded in a series of Legendre polynomials as

$$i(\tau,\mu)=\sum_{m=0}^{\infty}\frac{2m+1}{4\pi}P_m(\mu)\psi_m(\tau) \tag{6}$$

with functions $\psi_m(\tau)$ to be determined. Once $\psi_m(\tau)$ are known, i is completely defined by Eq. (6). Performing the derivation as outlined in Appendix A, we obtain

$$(m+1)\frac{\mathrm{d}\psi_{m+1}(\tau)}{\mathrm{d}\tau}+(m+1)(m+2)\frac{\psi_{m+1}(\tau)}{\tau}$$

$$+(2m+1)(1-\omega a_m)\psi_m(\tau)+m\frac{\mathrm{d}\psi_{m-1}(\tau)}{\mathrm{d}\tau}$$

$$-(m-1)m\frac{\psi_{m-1}(\tau)}{\tau}-(1-\omega)\left[\frac{\dot{Q}}{\sigma_a}+\psi_0(\tau)\right]\delta_{om}=0,$$

$$m=0,1,2\ldots \tag{7}$$

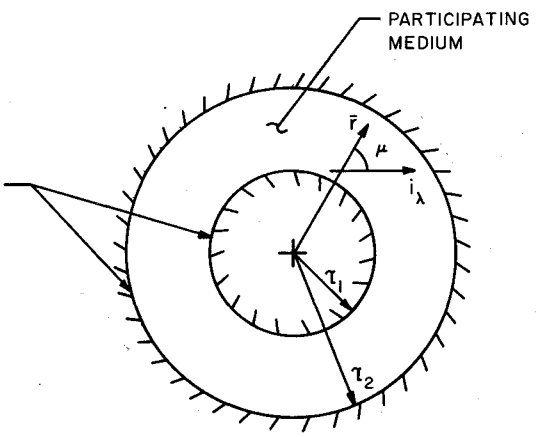

Fig. 1 Schematic of the physical system.

For the P-N approximation, $\psi_{N+1}(\tau)$ is assumed to be 0. Then there are $N+1$ linear coupled ordinary differential equations to be solved for $\psi_0(\tau)$, $\psi_1(\tau)$, . . . ,$\psi_N(\tau)$.

For practical calculations, the infinite series in the phase function (see Eq. 4) is terminated after a finite number of terms. Usually the number of terms retained depends on the level of mathematical complexity desired and the physical scattering phenomenon being modeled. However, in the spherical harmonics method, the order of approximation also limits the number of terms that can be carried in the phase function. For example, in the P-N approximation only $a_0,a_1,\ldots,a_N$ appear in the differential equations. Therefore, in the P-1 approximation, only the isotropic scattering and linear anisotropic scattering models can be represented; the Rayleigh scattering model requires at least the P-2 approximation (see Table 1).

The boundary conditions at the inner and outer spheres are respectively,

$$i(\tau_1)=\epsilon_1 i_{b1}+2(1-\epsilon_1)\int_0^1 i(\tau_1,-\mu')\mu'\mathrm{d}\mu',\qquad \mu'>0 \tag{8a}$$

Table 1 Values of a_j for different types of scattering

	Isotropic scattering	Rayleigh scattering	Linear-anisotropic scattering
a_0	1	1	1
a_1	0	0	Bounded between $-1/3$ and $1/3$ for f to remain positive at all angles
a_2	0	1/10	0
a_j, $j=3,4\ldots$	0	0	0

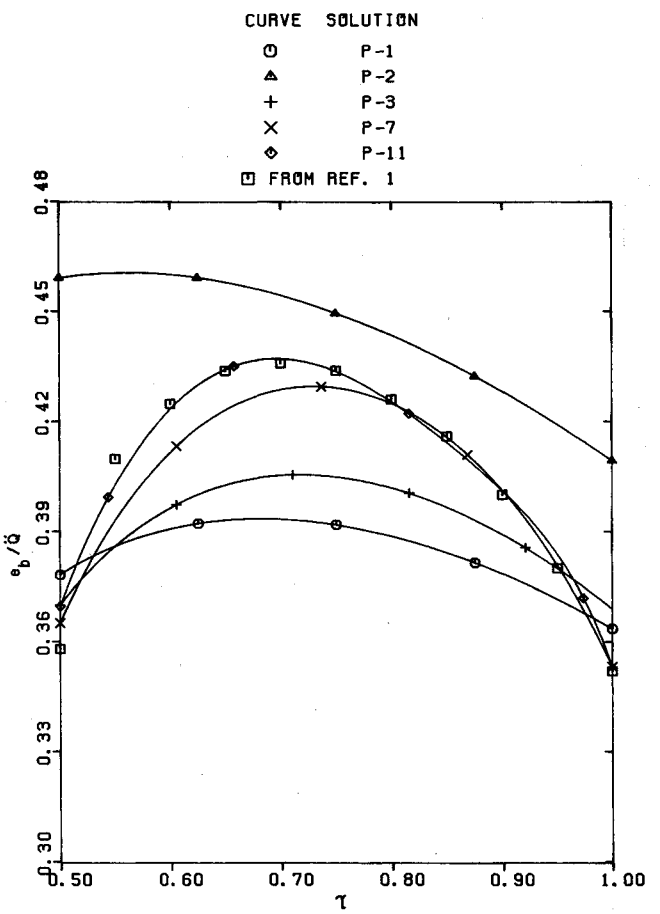

Fig. 2 Blackbody emissive power of the medium for $\omega=0$, $\tau_2=1$, and $\tau_1/\tau_2=0.5$.

Table 2 Wall heat fluxes ($\psi_1/\ddot{Q}$) for $\omega=0$

τ_2	τ_1/τ_2	Sparrow et al.[1]	P-1	P-2	P-3	P-7	P-11
				$\tau=\tau_1$(inner wall)			
0.1	0.05		−0.0355(−23)[a]	0.0014	−0.0538(16)	−0.0493(6)	−0.0463
	0.50	−0.0154	−0.0236(47)	0.0131	−0.0219(36)	−0.0179(11)	−0.0161
	0.75	−0.0087	−0.0124(22)	0.0169	−0.0099(−3)	−0.0096(−6)	−0.0102
	0.95	−0.0021	−0.0025(32)	0.0102	−0.0024(26)	−0.0022(16)	−0.0019
1.0	0.05		−0.542(11)	−0.206(−58)	−0.625(28)	−0.542(11)	−0.490
	0.50	−0.185	−0.256(39)	−0.067(64)	−0.224(22)	−0.200(9)	−0.184
	0.75	−0.096	−0.126(35)	−0.036(−61)	−0.106(14)	−0.102(10)	−0.093
	0.95	−0.021	−0.025(32)	−0.007(−63)	−0.024(26)	−0.022(16)	−0.019
10.0	0.05		−16.41(40)	−8.68(−26)	−13.6(16)	−12.4(6)	−11.7
	0.50		−3.08(5)	−2.96(−1)	−2.98(1)	−2.97(1)	−2.94
	0.75		−1.33(4)	−1.28(0)	−1.30(2)	−1.29(1)	−1.28
	0.95		−0.251(7)	−0.236(0)	−0.245(4)	−0.242(3)	−0.235
				$\tau=\tau_2$(outer wall)			
			0.0332(0)	0.0333(0)	0.0332(0)	0.0332(0)	0.0332
		0.0253	0.0233(−7)	0.0324(29)	0.0237(−6)	0.0247(−2)	0.0251
		0.0144	0.0123(−9)	0.0288(113)	0.0137(1)	0.0139(3)	0.0135
		0.0029	0.0025(−19)	0.0139(348)	0.0026(−16)	0.0028 (−10)	0.0031
			0.332(0)	0.333(0)	0.332(0)	0.332(0)	0.332
		0.245	0.228(−7)	0.275(12)	0.236(−4)	0.242(−2)	0.246
		0.138	0.122(−13)	0.172(23)	0.133(−5)	0.135(−4)	0.140
		0.028	0.025(−17)	0.042(40)	0.026(−13)	0.027(−10)	0.030
			3.29(0)	3.31(0)	3.29(0)	3.30(0)	3.30
			2.14(−2)	2.18(0)	2.17(0)	2.18(0)	2.18
			1.18(−2)	1.21(1)	1.20(0)	1.20(0)	1.20
			0.249(−5)	0.262(0)	0.254(−3)	0.257(−2)	0.263

[a]Numbers within parentheses are % differences when compared to the P-11 solution.

and

$$i(\tau_2)=\epsilon_2 i_{b2}+2(1-\epsilon_2)\int_0^1 i(\tau_2,\ \mu')\mu'\mathrm{d}\mu',\qquad \mu'>0 \quad (8b)$$

To be compatible with the spherical harmonic approximation, the boundary conditions must be reformulated. The moments of the intensity are required to be conserved instead of the intensity. Hence, the boundary conditions become

$$\int_0^1 i(\tau_1,\mu)\mu^n\mathrm{d}\mu = \int_0^1\left[\epsilon_1 i_{b1}+2(1-\epsilon_1)\int_0^1 i(\tau_1,-\mu')\mu'\mathrm{d}\mu'\right]\mu^n\mathrm{d}\mu,\ \mu>0 \quad (9a)$$

$$\int_0^1 i(\tau_2,-\mu)\mu^n\mathrm{d}\mu = \int_0^1\left[\epsilon_2 i_{b2}+2(1-\epsilon_2)\int_0^1 i(\tau_2,\mu')\mu'\mathrm{d}\mu'\right]\mu^n\mathrm{d}\mu,\ \mu>0 \quad (9b)$$

where n, consistent with the order of approximation, is obtained from Eq. (6). The values for n should be chosen so that sufficient boundary conditions are available to determine the integration constants. In the P-1 and P-2 approximations there are only two integration constants and $n=1$ would yield the required boundary conditions. In the P-3 solution, four integration constants need to be determined and $n=1$ and 3 are required.

Solutions

The unknown functions $\psi_0(\tau),\ \psi_1(\tau),\ \ldots,\psi_n(\tau)$ are related to the intensity by

$$\psi_m(\tau)=2\pi\int_{-1}^1 i(\tau,\mu)P_m(\mu)\mathrm{d}\mu \quad (10)$$

Substituting $m=0$ and $m=1$, we obtain

$$\psi_0(\tau)=2\pi\int_{-1}^1 i(\tau,\mu)\mathrm{d}\mu \quad (11)$$

$$\psi_1(\tau)=2\pi\int_{-1}^1 i(\tau,\mu)\mu\mathrm{d}\mu \quad (12)$$

It is seen that by definition $\psi_0(\tau)$ and $\psi_1(\tau)$ are the irradiance and the radiant heat flux, respectively. In the field of heat transfer it is usually these two quantities that are of interest rather than the intensity itself. Thus, only the solutions for $\psi_0(\tau)$ and $\psi_1(\tau)$ will be presented.

By setting $m=1$ in the P-1 approximation, two coupled first order ordinary differential equations (ODE) for $\psi_0(\tau)$ and $\psi_1(\tau)$ resulted from Eq. (7). Their solutions were obtained by first decoupling the ODE, then integrating the decoupled equations. The solutions are

$$\psi_0(\tau)=-\frac{(1-\omega)(1-\omega a_1)\ddot{Q}}{2}\tau^2+3(1-\omega a_1)\frac{F_1}{\tau}+F_2 \quad (13)$$

$$\psi_1(\tau)=\frac{(1-\omega)\ddot{Q}}{3}\tau+\frac{F_1}{\tau^2} \quad (14)$$

where

$$\ddot{Q}=\frac{\dot{Q}}{\sigma_a} \quad (15)$$

The integration constants F_1 and F_2 were determined through the use of Eqs. (6,), (9a), (9b), (13), and (14). Their expressions are given in Appendix B. In the P-2 approximation $m=2$

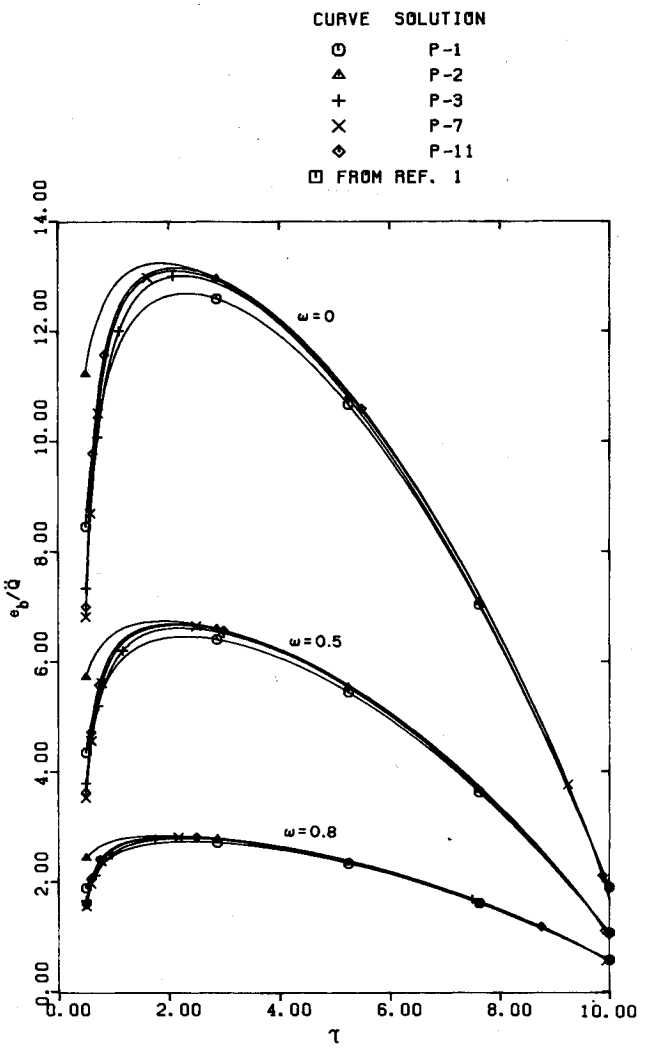

Fig. 3a Blackbody emissive power of the medium for $a_1 = 0$, $\tau_2 = 10$, and $\tau_1/\tau_2 = 0.05$.

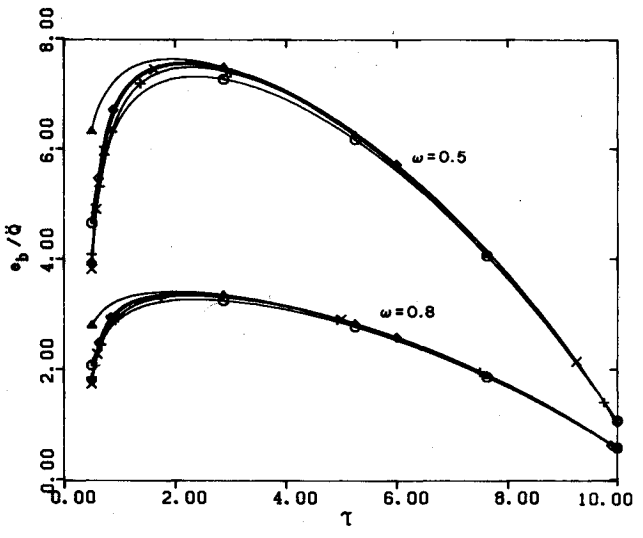

Fig. 3b Blackbody emissive power of the medium for $a_1 = -1/3$, $\tau_2 = 10$, and $\tau_1/\tau_2 = 0.05$.

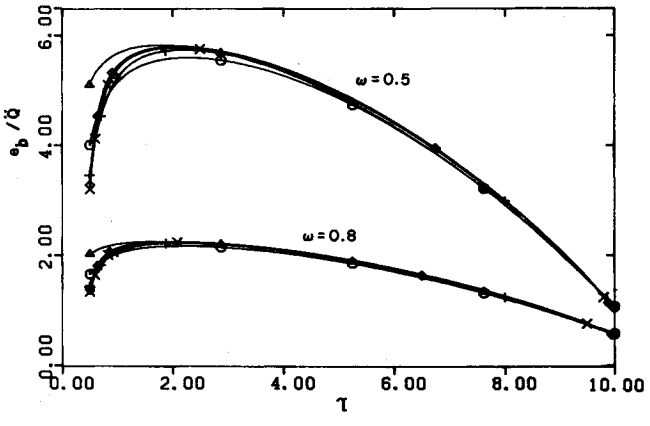

Fig. 3c Blackbody emissive power of the medium for $a_1 = 1/3$, $\tau_2 = 10$, and $\tau_1/\tau_2 = 0.05$.

and there are three first-order ODE governing $\psi_0(\tau)$, $\psi_1(\tau)$, and $\psi_2(\tau)$. Since only $\psi_0(\tau)$ and $\psi_1(\tau)$ are of interest, we present only their solutions.

$$\psi_0(\tau) = -\frac{(1-\omega)(1-\omega a_1)\ddot{Q}}{2}\tau^2 + 3(1-\omega a_1)\frac{G_1}{\tau} + 3G_2 \tag{16}$$

$$\psi_1(\tau) = \frac{(1-\omega)\ddot{Q}}{3}\tau + \frac{G_1}{\tau^2} \tag{17}$$

The integration constants G_1 and G_2 were similarly determined as in the P-1 approximation and their expressions are included in Appendix B.

Similarly, for the P-3 approximation, $m = 3$. Thus

$$\psi_0(\tau) = 3(1-\omega a_1)\left[\frac{H_1}{\tau} - \frac{(1-\omega)\ddot{Q}}{6}\tau^2\right] + \frac{6\xi\tau^{-1/2}}{5(1-\omega a_2)}\left[H_2 I_{1/2}(\xi\tau) - H_3 K_{1/2}(\xi\tau)\right] + H_4 \tag{18}$$

$$\psi_1(\tau) = \frac{(1-\omega)\ddot{Q}}{3}\tau + \frac{H_1}{\tau^2} \tag{19}$$

where

$$\xi = \left[\frac{35}{9}(1-\omega a_2)(1-\omega a_3)\right]^{1/2} \tag{20}$$

Four algebraic equations relating H_1, H_2, and H_4 can be obained by setting $n = 1$ and 3 in Eqs. (9a) and (9b) and by combining them with Eqs. (6), (18), and (19) and the following solutions for $\psi_2(\tau)$ and $\psi_3(\psi)$

$$\psi_2(\tau) = \frac{1}{5(1-\omega a_2)}\left\{\frac{6H_1}{\tau^3} - 3\xi\tau^{-1/2}\left[H_2 I_{5/2}(\xi\tau) - H_3 K_{5/2}(\xi\tau)\right]\right\} \tag{21}$$

$$\psi_3(\tau) = \tau^{-1/2}\left[H_2 I_{7/2}(\xi\tau) + H_3 K_{7/2}(\xi\tau)\right] + \frac{10H_1}{\xi^2\tau^4} \tag{22}$$

As the algebraic equations are rather long, we have simply solved them numerically for any given set of parameters instead of deriving the analytical expressions for each of the four integration constants.

The P-7 and P-11 solutions were obtained numerically using a FORTRAN computer code called "DVCPR" in the IMSL library. The code is designed for solving two-point boundary value problems involving a system of ordinary differential equations. It performs a finite-difference calculation using

Table 3 Wall heat fluxes ($\psi_1/\ddot{Q}$) for $\tau_2 = 0.1$ with scattering

ω	a_1	τ_1/τ_2	P-1	P-2	P-3	P-7	P-11
				$\tau=\tau_1$(inner wall)			
0.5	$-1/3,0,1/3$	0.05	$-0.018(-22)$[a]	0.0007	$-0.027(17)$	$-0.025(9)$	-0.023
		0.50	$-0.012(50)$	0.0065	$-0.011(38)$	$-0.009(13)$	-0.008
		0.75	$-0.0062(22)$	0.0085	$-0.0050(-2)$	$-0.0048(-6)$	-0.0051
		0.95	$-0.0012(33)$	0.0051	$-0.0012(33)$	$-0.0011(22)$	-0.0009
0.8	$-1/3,0,1/3$	0.05	$-0.007(-22)$	0.0003	$-0.011(22)$	$-0.010(11)$	-0.009
		0.50	$-0.0047(47)$	0.0026	$-0.0044(38)$	$-0.0036(13)$	-0.0032
		0.75	$-0.0025(25)$	0.0034	$-0.0020(0)$	$-0.0019(1)$	-0.0020
		0.95	$-0.0005(25)$	0.0020	$-0.0005(25)$	$-0.0004(0)$	-0.0004
				$\tau=\tau_2$(outer wall)			
			0.0166(0)	0.0167(0)	0.0166(0)	0.0166(0)	0.0166
			0.0116(−8)	0.0162(29)	0.0118(−6)	0.0123(−2)	0.0126
			0.0062(−9)	0.0144(111)	0.0068(0)	0.0069(0)	0.0068
			0.0012(−20)	0.0070(367)	0.0013(−13)	0.0014(−7)	0.0015
			0.0066(0)	0.0067(0)	0.0066(0)	0.0066(0)	0.0066
			0.0057(14)	0.0065(30)	0.0047(−6)	0.0049(−2)	0.0050
			0.0025(−7)	0.0057(111)	0.0027(0)	0.0028(4)	0.0027
			0.0005(17)	0.0028(367)	0.005(−17)	0.0006(0)	0.0006

[a]Numbers within parentheses are % differences when compared to the P-11 solution.

adaptive mesh sizes. The convergence criterion in all of the calculations was chosen such that a relative tolerance of no greater than 10^{-3} was met at all mesh points.

Numerical Results and Discussion

The numerical results in this section that were generated from the solutions presented in the preceding section are given and compared. The numerical results include the radiant heat flux ψ_1 evaluated at the inner and outer walls of the spherical enclosure, and the blackbody emissive power of the medium e_b, which is related to ψ_0. The wall heat fluxes are presented in dimensionless form defined by $\psi_1/\ddot{Q}$. The blackbody emissive power of the medium is also given in dimensionless form and it can be obtained from Eqs. (5) and (11) as

$$e_b(T)/\ddot{Q} = [1+\psi_0(\tau)/\ddot{Q}]/4 \tag{23}$$

where e_b has been used to replace πi_b in the derivation. It should be mentioned that by virtue of Stefan-Boltzmann's law, knowing e_b is equivalent to knowing the temperature distribution in the medium.

The wall heat fluxes presented are for the case where both the inner and outer walls are black and held at a common temperature. In addition to these assumptions, the common wall temperature was assumed zero in generating the results for the blackbody emissive power of the medium.

Wall Heat Fluxes

Table 2 gives the wall heat fluxes for the case of no scattering of radiation by the medium (i.e., $\omega=0$). Tables 3, 4, and 5 are for non-zero ω, but different τ_2. The medium is optically thin when either $\tau_2 \ll 1$ or $\tau_1/\tau_2 \to 1$, and is optically thick when $\tau_2 \gg 1$ and τ_1/τ_2 is not approaching 1. The numbers within the parentheses are the percent differences when compared to the P-11 solution. The results are converging as the order of the P-N approximation is increased. The lower order solutions converge faster at the outer wall than at the inner wall. Differences as large as -17% and -10% still can exist for the P-3 and P-7 solutions, respectively, at the outer wall. At the inner wall, the largest differences for the P-3 and P-7 solutions are 38% and 22%, respectively. Only at the outer wall, when either $\tau_1/\tau_2 \to 0$ or $\tau_2 = 10$, can the lower order solutions always be considered good approximations of the P-11 solution. Apart from these conditions, the accuracy of the lower order solutions depends on the specific values of τ_1/τ_2 and τ_2. As noted by Pomraning,[5] the P-2 solution yielded the same boundary heat fluxes as the P-1 solution for solid spherical systems. The results in Tables 2 through 5 indeed indicate that as $\tau_1/\tau_2 \to 0$ (i.e., the system becomes a solid sphere) the outer wall P-1 and P-2 results approach each other. When $\tau_2 = 10$, the P-2 solution approximates the higher order solutions more accurately than the P-1 solution at both walls. However, the opposite is true when $\tau_2 = 0.1$ and 1 except at the outer wall and in the limit $\tau_1/\tau_2 \to 0$. Moreover, when $\tau_2 = 0.1$, the P-2 solution fails to correctly predict the direction of heat flow at the inner wall.

For $\omega = 0$, the exact results from Sparrow et al.[1] are also included in Table 2. In general, the P-N results are converging toward the exact results. As ω increases, the wall heat fluxes decreases. For example, when ω increases from 0 to 0.5, the wall heat fluxes decrease by roughly 50% (compare Sparrow et al.'s results in Table 2 to the P-11 results in Table 3).

The type of scattering considered in Tables 3, 4, and 5 is linear anisotropic scattering, and the angular distribution coefficients a_j in Eq. (4) are as defined in Table 1. The values $-1/3$, 0, $1/3$ used for a_1 in the calculation correspond to strong backward, isotropic, and strong forward scattering, respectively. The results in Table 3 show that the wall heat fluxes are the same no matter what a_1 is. This is because for $\tau_2 = 0.1$, the medium is optically thin and the transport of radiant energy is independent of the type of scattering in the medium. Tables 4 and 5 are for $\tau_2 = 1$ and 10, respectively. The type of scattering is now beginning to have some effect on the wall heat fluxes. The heat flux increases at the inner wall as the medium scatters radiation more strongly in the backward direction, and it is the opposite at the outer wall. When $\tau_1/\tau_2 \to 1$, however, the effect is minimal as the medium again approaches the optically thin limit.

In both Tables 2 and 5 the inner and outer wall heat fluxes are quite close to each other for $\tau_2 = 10$ and $\tau_1/\tau_2 = 0.75$ and 0.95. This is not surprising since in the limit $\tau_1/\tau_2 \to 1$ when $\tau_2 \gg 1$ the spherical medium becomes a planar medium and the wall heat fluxes should be identical.

Table 4 Wall heat fluxes ($\psi_1/\ddot{Q}$) for $\tau_2 = 1$ with scattering

ω	a_1	τ_1/τ_2	P-1	P-2	P-3	P-7	P-11
					$\tau=\tau_1$(inner wall)		
0.5	−1/3	0.05	−0.2869(12)[a]	−0.0116(−95)	−0.3272(27)	−0.2847(11)	−0.2573
		0.50	−0.1296(37)	−0.0365(−61)	−0.1137(21)	−0.1017(18)	−0.0943
		0.75	−0.0630(34)	−0.0190(−60)	−0.0535(14)	−0.0516(10)	−0.0470
		0.95	−0.0125(29)	−0.0033(−66)	−0.0119(23)	−0.0112(15)	−0.0097
	0	0.05	−0.2707(11)	−0.0103(−96)	−0.3126(28)	−0.2713(11)	−0.2449
		0.50	−0.1282(39)	−0.0337(−63)	−0.1121(22)	−0.0998(8)	−0.0922
		0.75	−0.0629(35)	−0.0180(−61)	−0.0532(14)	−0.0512(10)	−0.0466
		0.95	−0.0125(29)	−0.0033(−66)	−0.0119(23)	−0.0112(15)	−0.0097
	1/2	0.05	−0.2543(10)	−0.0090(−96)	−0.2977(27)	−0.2576(11)	−0.2322
		0.50	−0.1267(41)	−0.0308(−66)	−0.1103(22)	−0.0977(8)	−0.0901
		0.75	−0.0627(36)	−0.0170(−63)	−0.0529(15)	−0.0508(10)	−0.0461
		0.95	−0.0125(30)	−0.0032(−67)	−0.0119(23)	−0.0112(17)	−0.0096
0.8	−1/3	0.05	−0.1185(12)	−0.0049(−95)	−0.1343(27)	−0.1171(11)	−0.1059
		0.50	−0.0522(37)	−0.0152(−60)	−0.0459(20)	−0.0411(8)	−0.0382
		0.75	−0.0252(33)	−0.0078(−59)	−0.0215(14)	−0.0207(10)	−0.0189
		0.95	−0.0050(28)	−0.0013(−67)	−0.0048(23)	−0.0044(13)	−0.0039
	0	0.05	−0.1083(11)	−0.0041(−96)	−0.1250(27)	−0.1085(11)	−0.0980
		0.50	−0.0513(39)	−0.0135(−63)	−0.0448(21)	−0.0399(8)	−0.0369
		0.75	−0.0251(35)	−0.0072(−61)	−0.0213(15)	−0.0205(10)	−0.0186
		0.95	−0.0050(28)	−0.0013(−67)	−0.0048(23)	−0.0044(13)	−0.0039
	1/3	0.05	−0.0977(9)	−0.0033(−96)	−0.1154(29)	−0.1000(11)	−0.0898
		0.50	−0.0503(42)	−0.0116(−67)	−0.0437(23)	−0.0386(9)	−0.0355
		0.75	−0.0250(37)	−0.0065(−64)	−0.0210(15)	−0.0202(10)	−0.0183
		0.95	−0.0050(28)	−0.0013(−67)	−0.0048(23)	−0.0045(15)	−0.0039
					$\tau=\tau_2$(outer wall)		
			0.1659(0)	0.1666(0)	0.1658(0)	0.1659(0)	0.1660
			0.1134(−8)	0.1367(12)	0.1174(−4)	0.1204(−2)	0.1223
			0.0609(−13)	0.0857(23)	0.0663(−5)	0.0673(−4)	0.0699
			0.0125(−17)	0.0208(39)	0.0130(13)	0.0137(−9)	0.0150
			0.1660(0)	0.1666(0)	0.1659(0)	0.1660(0)	0.1660
			0.1138(−7)	0.1374(12)	0.1178(−4)	0.1209(−2)	0.1228
			0.0610(−13)	0.0862(23)	0.0665(−6)	0.0675(−4)	0.0702
			0.0125(−17)	0.0208(38)	0.0130(−14)	0.0137(−9)	0.0151
			0.1660(0)	0.1666(0)	0.1659(0)	0.1660(0)	0.1661
			0.1142(−7)	0.1381(12)	0.1182(−4)	0.1214(−2)	0.1233
			0.0611(−13)	0.0868(23)	0.0667(−5)	0.0678(−4)	0.0704
			0.0125(−17)	0.0209(38)	0.0130(−14)	0.0137(−9)	0.0151
			0.0664(0)	0.0666(0)	0.0663(0)	0.0664(0)	0.0664
			0.0453(−7)	0.0545(12)	0.0469(−4)	0.0481(−1)	0.0488
			0.0243(−13)	0.0341(22)	0.0265(−5)	0.0269(−4)	0.0279
			0.0050(−17)	0.0083(38)	0.0052(−13)	0.0055(−8)	0.0060
			0.0664(0)	0.0667(0)	0.0664(0)	0.0664(0)	0.0664
			0.0455(−7)	0.0550(12)	0.0471(−4)	0.0484(−1)	0.0491
			0.0244(−13)	0.0345(23)	0.0266(−5)	0.0270(−4)	0.0281
			0.0050(−17)	0.0083(38)	0.0052(−13)	0.0055(−8)	0.0060
			0.0664(0)	0.0667(0)	0.0664(0)	0.0664(0)	0.0664
			0.0458(−7)	0.0554(12)	0.0474(−4)	0.0487(−2)	0.0495
			0.0245(−13)	0.0349(24)	0.0267(−5)	0.0272(−4)	0.0282
			0.0050(−17)	0.0084(38)	0.0052(−13)	0.0055(−8)	0.0060

[a]Numbers within parentheses are % differences when compared to the P-11 solution.

Blackbody Emissive Power of the Medium

The blackbody emissive power of the medium for $\omega = 0$, $\tau_2 = 1$ and $\tau_1/\tau_2 = 0.5$ is illustrated in Fig. 2. The maximum deviation from the exact profile is about 10% for the P-1 solution and approximately 7% for the P-3 solution. The deviation for the P-7 and P-11 solutions are substantially smaller and can be considered as excellent approximations of the exact profile. The P-2 solution does not yield a close approximation of the exact profile.

In Figs. 3a, 3b, and 3c is a series of plots of $e_b/\ddot{Q}$ for $\tau_2 = 10$, $\tau_1/\tau_2 = 0.05$, different ω and a_1. The results from all of the different orders of approximation are quite close to each other except for the P-2 profile at the inner wall. The figures show that as ω increases, $e_b/\ddot{Q}$ in the entire medium decreases, and $e_b/\ddot{Q}$ increases in the direction from forward to backward scattering.

In all the plots for $e_b/\ddot{Q}$, there is a peak that is closer to the inner wall than to the outer wall. The peak is equivalent to the maximum temperature in the medium. Making a comparison

Table 5 Wall heat fluxes ($\psi_1/\ddot{Q}$) for $\tau_2 = 10$ with scattering

ω	a_1	τ_1/τ_2	P-1	P-2	P-3	P-7	P-11
					$\tau=\tau_1$(inner wall)		
0.5	−1/3	0.05	−8.804(37)[a]	−4.805(−25)	−7.392(15)	−6.743(5)	−6.408
		0.50	−1.556(4)	−1.501(1)	−1.509(1)	−1.503(1)	−1.489
		0.75	−0.670(4)	−0.647(1)	−0.652(1)	−0.650(1)	−0.643
		0.95	−0.126(7)	−0.119(1)	−0.123(4)	−0.121(3)	−0.118
	0	0.05	−8.207(40)	−4.340(−26)	−6.820(16)	−6.190(6)	−5.867
		0.50	−1.542(5)	−1.481(1)	−1.490(1)	−1.483(1)	−1.468
		0.75	−0.666(4)	−0.642(1)	−0.648(2)	−0.645(1)	−0.638
		0.95	−0.126(8)	−0.118(1)	−0.123(5)	−0.121(3)	−0.117
	1/3	0.05	−7.522(43)	−3.838(−27)	−6.179(17)	−5.577(6)	−5.270
		0.50	−1.524(6)	−1.455(1)	−1.465(2)	−1.458(1)	−1.441
		0.75	−0.663(5)	−0.635(1)	−0.642(2)	−0.639(1)	−0.631
		0.95	−0.125(7)	−0.118(1)	−0.122(4)	−0.121(3)	−0.117
0.8	−1/3	0.05	−3.650(36)	−2.028(−24)	−3.082(15)	−2.820(5)	−2.684
		0.50	−0.625(4)	−0.605(1)	−0.607(1)	−0.605(1)	−0.600
		0.75	−0.268(3)	−0.260(0)	−0.261(1)	−0.261(1)	−0.259
		0.95	−0.050(6)	−0.047(0)	−0.049(4)	−0.049(4)	−0.047
	0	0.05	−3.283(40)	−1.736(−26)	−2.728(16)	−2.476(5)	−2.347
		0.50	−0.617(5)	−0.592(1)	−0.596(2)	−0.593(1)	−0.587
		0.75	−0.267(5)	−0.257(1)	−0.259(2)	−0.258(1)	−0.255
		0.95	−0.050(6)	−0.047(0)	−0.049(4)	−0.048(0)	−0.047
	1/3	0.05	−2.824(45)	−1.407(−28)	−2.302(18)	−2.070(6)	−1.953
		0.50	−0.604(6)	−0.574(1)	−0.579(2)	−0.576(1)	−0.568
		0.75	−0.264(5)	−0.252(0)	−0.255(2)	−0.254(1)	−0.251
		0.95	−0.050(6)	−0.047(0)	−0.049(4)	−0.048(2)	−0.047
					$\tau=\tau_2$(outer wall)		
			1.644(0)	1.654(0)	1.648(0)	1.650(0)	1.650
			1.069(−2)	1.083(0)	1.081(0)	1.083(0)	1.086
			0.587(−2)	0.600(0)	0.597(−1)	0.598(1)	0.602
			0.124(−5)	0.131(0)	0.127(−3)	0.128(−2)	0.131
			1.656(0)	1.656(0)	1.649(0)	1.651(0)	1.652
			1.073(−2)	1.088(0)	1.086(0)	1.088(0)	1.091
			0.589(−3)	0.603(0)	0.599(−1)	0.601(−1)	0.605
			0.124(−6)	0.131(0)	0.127(−4)	0.128(−3)	0.132
			1.648(0)	1.657(0)	1.651(0)	1.652(0)	1.653
			1.077(−2)	1.095(0)	1.092(−1)	1.094(0)	1.098
			0.590(−3)	0.606(0)	0.602(−1)	0.604(−1)	0.608
			0.124(−6)	0.131(0)	0.127(−4)	0.129(−3)	0.132
			0.658(0)	0.662(0)	0.659(0)	0.660(0)	0.660
			0.427(−1)	0.432(0)	0.432(0)	0.432(0)	0.433
			0.235(−2)	0.239(0)	0.238(−1)	0.239(0)	0.240
			0.050(−4)	0.052(0)	0.051(−2)	0.051(−2)	0.052
			0.658(0)	0.662(0)	0.660(0)	0.660(0)	0.661
			0.429(−2)	0.435(0)	0.434(−1)	0.435(0)	0.437
			0.235(−3)	0.241(0)	0.240(−1)	0.240(−1)	0.242
			0.050(−6)	0.052(−2)	0.051(−4)	0.051(−4)	0.053
			0.660(0)	0.663(0)	0.661(0)	0.661(0)	0.662
			0.432(−2)	0.440(0)	0.439(0)	0.439(0)	0.441
			0.237(−3)	0.244(0)	0.242(−1)	0.243(0)	0.244
			0.050(−6)	0.053(0)	0.051(−4)	0.052(−2)	0.053

[a]Numbers within parentheses are % differences when compared to the P-11 solution.

of Fig. 2 and Figs. 3a, 3b, and 3c, one can see that the peak moves toward the inner wall as $\tau_1/\tau_2 \to 0$. As pointed out before, in the limit $\tau_1/\tau_2 \to 0$, the concentric-sphere system reduces to that of a solid sphere. Because of symmetry, the maximum temperature for such a geometry must be exactly at the center.

Conclusions

The problem of radiative heat transfer in emitting-absorbing-scattering media contained in a concentric spherical enclosure was studied in this work. Linear anisotropic scattering was assumed. The spherical harmonics method was used to solve the equation of transfer. Analytical solutions were obtained for the P-1, P-2, and P-3 approximations, while finite-difference numerical results were obtained for the P-7 and P-11 approximations.

It was found that all the wall heat flux results converged as the order of approximation was increased. The lower order approximations converged faster at the outer wall than at the inner wall. At the outer wall, and when either $\tau_1/\tau_2 \to 0$ or

$\tau_2 = 10$, the lower order solutions were always close approximations of the P-11 solution. Except for these conditions, the accuracy of the lower order solutions varied widely depending on the specific values of τ_1/τ_2 and τ_2. For $\tau_2 = 0.1$, the P-2 approximation gave erroneous results at the inner wall in that it did not predict the correct direction of energy flow. For $\tau_2 = 10$, the P-2 results were more accurate than the P-1 results. The P-2 approximation, however, was found incapable of giving accurate approximations of the blackbody emissive power distribution in the medium for any of the τ_2 values considered.

It was also determined that scattering had the effect of lowering the wall heat fluxes. The type of scattering did not have any appreciable effects on the heat fluxes when the medium was optically thin. For optically intermediate and thick media, heat fluxes at the inner and outer walls increased and decreased, respectively, as the media scattered radiation more strongly in the backward direction. In addition, strong backward scattering also resulted in higher blackbody emissive power in the medium.

Appendix A

Substituting Eqs. (4) and (6) into Eq. (1), utilizing the orthogonality of Legender polynomials

$$\int_{-1}^{1} P_j(\mu)P_m(\mu)\mathrm{d}\mu = \begin{cases} 0 & m \neq j \\ \dfrac{2}{2m+1} & m = j \end{cases} \tag{A1}$$

and the following recurrence formula

$$\mu P_m(\mu) = \frac{(m+1)P_{m+1}(\mu) + mP_{m-1}(\mu)}{(2m+1)} \tag{A2}$$

$$(1-\mu^2)\frac{\mathrm{d}P_m(\mu)}{\mathrm{d}\mu} = mP_{m-1}(\mu) - m\mu P_m(\mu) \tag{A3}$$

yields

$$\sum_{m=0}^{\infty} \left\{ (m+1)\frac{\mathrm{d}\psi_{m+1}(\tau)}{\mathrm{d}\tau} + (m+1)(m+2)\frac{\psi_{m+1}(\tau)}{\tau} + (2m+1)(1-\omega a_m)\psi_m(\tau) + m\frac{\mathrm{d}\psi_{m-1}(\tau)}{\mathrm{d}\tau} - (m-1)m\frac{\psi_{m-1}(\tau)}{\tau} - 4\pi(1-\omega)i_b(T)\delta_{om} \right\} P_m(\mu) = 0 \tag{A4}$$

where the relation

$$\psi_m(\tau) = 2\pi\int_{-1}^{1} i(\tau,\mu)P_m(\mu)\mathrm{d}\mu \tag{A5}$$

has been used. Equation (A4) is valid for arbitrary μ if and only if the coefficients of $P_m(\mu)$ vanish identically. Thus

$$(m+1)\frac{\mathrm{d}\psi_{m+1}(\tau)}{\mathrm{d}\tau} + (m+1)(m+2)\frac{\psi_{m+1}(\tau)}{\tau} + (2m+1)(1-\omega a_m)\psi_m(\tau) + m\frac{\mathrm{d}\psi_{m-1}(\tau)}{\mathrm{d}\tau} - (m-1)m\frac{\psi_{m-1}(\tau)}{\tau} - 4\pi(1-\omega)i_b(\tau)\delta_{om} = 0, \quad m = 0,1,2\ldots \tag{A6}$$

Equations (5) and (A6) can be combined to give Eq. (7).

Appendix B: Integration Constants

(1) P-1 solution:

$$F_1 = \frac{C_3C_5 - C_2C_6}{C_1C_5 - C_2C_4}$$

$$F_2 = \frac{C_1C_6 - C_3C_4}{C_1C_5 - C_2C_4}$$

where

$$C_1 = \frac{3(1-\omega a_1)}{4\tau_1} + \left(\frac{1}{\epsilon_1} - \frac{1}{2}\right)\frac{1}{\tau_1^2}, \quad C_2 = \frac{1}{4}$$

$$C_3 = (1-\omega)\ddot{Q}\left[\frac{(1/2 - 1/\epsilon_1)\tau_1}{3} + \frac{(1-\omega a_1)\tau_1^2}{8}\right] + \pi i_{b1}$$

$$C_4 = \frac{3(1-\omega a_1)}{4\tau_2} + \left(\frac{1}{2} - \frac{1}{\epsilon_2}\right)\frac{1}{\tau_2^2}, \quad C_5 = \frac{1}{4}$$

$$C_6 = (1-\omega)\ddot{Q}\left[\frac{(1/\epsilon_2 - 1/2)\tau_2}{3} + \frac{(1-\omega a_1)\tau_2^2}{8}\right] + \pi i_{b2}$$

(2) P-2 solution:

$$G_1 = \frac{D_3D_5 - D_2D_6}{D_1D_5 - D_2D_4}$$

$$F_2 = \frac{D_1D_6 - D_3D_4}{D_1D_5 - D_2D_4}$$

where

$$D_1 = \frac{3(1-\omega a_1)}{4\tau_1} + \left(\frac{1}{\epsilon_1} - \frac{1}{2}\right)\frac{1}{\tau_1^2} + \frac{3}{8(1-\omega a_2)\tau_1^3}$$

$$D_2 = \frac{3}{4}$$

$$D_3 = (1-\omega)\ddot{Q}\left[\frac{(1/2 - 1/\epsilon_1)\tau_1}{3} + \frac{(1-\omega a_1)\tau_1^2}{8}\right] + \pi i_{b1}$$

$$D_4 = \frac{3(1-\omega a_1)}{4\tau_2} + \left(\frac{1}{2} - \frac{1}{\epsilon_2}\right)\frac{1}{\tau_2^2} + \frac{3}{8(1-\omega a_2)\tau_2^3}$$

$$D_5 = \frac{3}{4}$$

$$D_6 = (1-\omega)\ddot{Q}\left[\frac{(1/\epsilon_2 - 1/2)\tau_2}{3} + \frac{(1-\omega a_1)\tau_2^2}{8}\right] + \pi i_{b2}$$

Acknowledgment

This work was supported by the National Science Foundation through Grant DME-8105951.

References

[1]Sparrow, E.M., Usiskin, C.M., and Hubbard, H.A., "Radiation Heat Transfer in a Spherical Enclosure Containing a Participating, Heat-Generating Gas," *Journal of Heat Transfer,* Vol. 83, May 1961, pp. 199–206.

[2]Rhyming, I.L., "Radiative Transfer Between Two Concentric Spheres Separated by an Absorbing and Emitting Gas," *International Journal of Heat and Mass Transfer,* Vol. 9, April 1966, pp. 315–324.

[3]Dennar, E.A. and Sibulkin, M., "An Evaluation of the Differential Approximation for Spherically Symmetric Radiative Transfer," *Journal of Heat Transfer,* Vol. 91, Feb. 1969, pp. 73–76.

[4]Bayazitoglu, Y., and Higenyi, J., "Higher-Order Differential Equations of Radiative Transfer: P_3 Approximation," *AIAA Journal,* Vol. 17, April 1979, pp. 424–431.

[5]Pomraning, G.C., "Radiative Transfer via Spherical Harmonics," *Transport Theory and Statistical Physics,* Vol. 8, 1979, pp. 67–97.

[6]Yuen, W.W. and Tien, C.L., "Approximate Solutions of Radiative Transfer in One-Dimensional Non-Planar Systems, *Journal of Quantitative Spectroscopy and Radiative Transfer,* Vol. 19, May 1978, pp. 533-549.